Nanoscale

PAPER

Molecular recognition with nanostructures fabricated by photopolymerization within metallic subwavelength apertures†

Cite this: *Nanoscale*, 2014, **6**, 8656

J. L. Urraca,[ab] C. A. Barrios,*[c] V. Canalejas-Tejero,[c] G. Orellana*[d] and M. C. Moreno-Bondi*[a]

Received 28th February 2014
Accepted 14th May 2014

DOI: 10.1039/c4nr01129e

www.rsc.org/nanoscale

The first demonstration of fabrication of submicron lateral resolution molecularly imprinted polymer (MIP) patterns by photoinduced local polymerization within metal subwavelength apertures is reported. The size of the photopolymerized MIP features is finely tuned by the dose of 532 nm radiation. Rhodamine 123 (R123) has been selected as a fluorescent model template to prove the recognition capability of the MIP nanostructures, which has been evaluated by fluorescence lifetime imaging microscopy (FLIM) with single photon timing measurements. The binding selectivity provided by the imprinting effect has been confirmed in the presence of compounds structurally related to R123. These results pave the way to the development of nanomaterial architectures with biomimetic artificial recognition properties for environmental, clinical and food testing.

Introduction

Polymerization at the nanoscale is a subject of considerable interest in the field of molecularly imprinted polymers (MIPs). MIPs are tailor-made materials showing selective recognition to a template molecule present during the polymerization process.[1] These materials can be used as synthetic receptors in (bio)molecular sensing applications. Structuring MIPs at the micro- and nano-scale increases the recognition surface available, greatly improving the site accessibility of imprinted materials.[2] Implementation of MIP-based nanosensor architectures requires the formation of MIP micro- and nano-features with well-defined morphologies onto the surface of particular devices (*e.g.* transducers) and/or planar substrates (*e.g.* Si wafers). In this regard, different methods for MIP micro/nanostructuring have been demonstrated. For example, UV,[3] evanescent wave[4] and microstereo lithographic techniques[5] were used to synthesize MIP features with microscale lateral resolution. To achieve sub-micron lateral resolution, nanoimprint lithography was shown to be successful;[6] however, it requires a mould or stamp contacting the pre-polymerization mixture, which may contaminate the resulting MIP surface. We have recently reported the application of electron beam lithography (EBL) to the direct patterning of MIP nano-features on silicon substrates using a cross-linkable linear copolymer which behaves as both, a functional recognition material and an EBL resist.[7]

Nanophotonic devices offer a powerful means to achieve high optical confinement at the nanoscale. Some of them are capable to confine and enhance the optical field within low refractive index nanoregions, a feature that is particularly useful in applications such as biochemical sensing and nanolithography. For instance, plasmonic nanostructures such as metal nanoparticles and optical antennas can produce enhanced optical fields highly localized at their surfaces. This effect has been successfully applied to ultrahigh sensitivity optical biosensing[8,9] and nanometer-scale photopolymerization.[10–12] Metallic subwavelength apertures (MSAs)[13] are particularly appealing because of their geometrical simplicity and the possibility of being reliably and uniformly mass-produced through lithographic means,[14,15] allowing massive parallelism. An outstanding demonstration of light confinement inside MSAs was the achievement of single molecule detection by fluorescence correlation spectroscopy at biologically relevant concentrations.[16]

In this paper, we demonstrate for the first time the fabrication of MIP patterns with sub-micrometer lateral resolution by

[a]*Chemical Optosensors and Applied Photochemistry Group (GSOLFA), Department of Analytical Chemistry, Faculty of Chemistry, Universidad Complutense de Madrid, CEI Moncloa, 28040 Madrid, Spain. E-mail: mcmbondi@ucm.es*

[b]*CEI Moncloa, UCM-UPM, Avda Complutense s/n, E-28040 Madrid, Spain*

[c]*Instituto de Sistemas Optoelectrónicos y Microtecnología (ISOM), ETSI Telecomunicación, Universidad Politécnica de Madrid, CEI Moncloa, 28040 Madrid, Spain. E-mail: carlos.angulo.barrios@upm.es*

[d]*Chemical Optosensors and Applied Photochemistry Group (GSOLFA), Department of Organic Chemistry, Faculty of Chemistry, Universidad Complutense de Madrid, CEI Moncloa, 28040 Madrid, Spain. E-mail: orellana@quim.ucm.es*

† Electronic supplementary information (ESI) available: Fig. SI.1: chemical structure and acronyms of the different fluorescent dyes; optimization of polymer composition; Table SI.1. Template recovery after polymerization; determination of the binding capacity by equilibrium rebinding analysis; calculation of the propagation length of surface plasmon polariton (SPP) at the aluminum/pre-polymerization mixture interface at 532 nm wavelength. See DOI: 10.1039/c4nr01129e

photoinduced local polymerization within MSAs. The MSAs consist of small holes in an aluminum film deposited onto a microscope coverslip. The employed polymerizable formulation includes a photoinitiator that enables polymerization at 532 nm, and rhodamine 123 (R123) as a model template molecule, the fluorescence of which allows sensitive detection of the binding event. The size of the photopolymerized MIP features is determined and controlled by the dose of green radiation. The fabricated MIP nanostructures are structurally characterized as a function of the irradiation dosage and their recognition capability is evaluated through fluorescence lifetime imaging microscopy (FLIM) with single photon timing measurements of the bound R123 fluorescence.

Experimental

Reagents and materials

Rhodamine 123 (R123), rhodamine 6G (R6G) and fluorescein (FLU) (Fig. SI.1†) were supplied by Acros (Geel, Belgium). Methacrylic acid (MAA) and trifluoroacetic acid (TFA) (HPLC grade, 99%) were from Fluka (Buchs, Switzerland). The sensitizer dye Eosin Y (EY), 2′,4′,5′,7′-tetrabromofluorescein disodium salt, methyldiethanolamine (MDEA), ethylene glycol dimethacrylate (EDMA) and HEPES buffer were obtained from Sigma-Aldrich (St. Louis, MO, USA). HPLC grade acetonitrile (AcN) and methanol (MeOH) were purchased from SDS (Peypin, France) and water was purified with a Milli-Q system (Millipore, Bedford, MA). All solutions prepared for HPLC were passed through a 0.45 μm nylon filter before use.

HPLC-UV analysis

The chromatographic system consisted of a HP-1200 series high performance liquid chromatograph (HPLC) from Agilent Technologies (Palo Alto, CA, USA) equipped with a quaternary pump, on-line degasser, autosampler, automatic injector, column thermostat, and diode-array (DAD) detector. HPLC quantification of the dyes was performed on an Excel 2 C_{18}-PFP (2) (100 × 2.1 mm, 2 μm) column from ACE (Aberdeen, Scotland). The mobile phase consisted of a mixture of 40% AcN (by volume) and 60% water containing 0.1% TFA. The analyses were performed at a flow rate of 0.4 mL min^{-1} and the column temperature was kept at 40 °C. The injection volume was 10 μL and all the dyes were eluted within 10 min. The UV-VIS absorption detector was set at 510 nm. For quantification purposes, calibration standards were prepared by diluting in the mobile phase an adequate amount of the 200 mg L^{-1} dye stock solution in DMSO. All measurements were carried out in triplicate.

Equilibrium rebinding experiments

A series of MIP and non-imprinted polymer (NIP) samples (10 mg each) were weighed separately and taken into 1.5 mL HPLC glass vials. Then, 1 mL acetonitrile solutions containing increasing concentrations of R123 (0.003 mM to 2 mM) were added to each vial and the vials were shaken for 24 h at room temperature. After incubation, the amount of free R123 (F) remaining in the supernatant was determined by HPLC using the method described in the section LC-UV analysis. The amount of bound analyte to the polymer (B) was calculated by subtracting the non-bound amount (F) from the initial concentration in the solution.

For cross-selectivity evaluation the polymers (10 mg, MIP or NIP) were incubated with 1 mL acetonitrile solutions containing increasing concentrations of R6G or fluorescein (0.003 mM to 2 mM). After 24 h shaking, the concentration of dye in the supernatant was determined by HPLC-FLD and the experimental data were fitted to a Freundlich isotherm model (see ESI†).

Fabrication of metallic subwavelength aperture arrays

Glass substrates 1 mm thick were thoroughly washed with detergent in an ultrasonic bath and cleaned at 130 °C using piranha solution (H_2SO_4 96%–H_2O_2 30% 3 : 1 v/v), then rinsed with deionized water (DIW) and isopropyl alcohol, blown-dry with N_2 flow and heated at 100 °C for 10 min. Then, aluminum was deposited on the glass substrates by electron-beam evaporation at a deposition rate of 1 nm s^{-1}. The final film thickness was determined to be 92 nm using an Alpha-Step IQ surface profilometer. Next, a ZEP-520 positive tone EBL resist was spin-coated on the Al film at 5000 rpm and immediately baked for 10 min at 120 °C, resulting in a resist thickness of approximately 100 nm. 5 μm-period dot arrays were patterned in the resist film by e-beam single-shot exposure using a Crestec CABL-9000C high resolution EBL system (50 keV acceleration voltage, 1 nA beam current, 200 μs exposure time). The exposed resist was developed at 0 °C for 40 s and then dried under a N_2 flow. Inductively coupled plasma (ICP) chemical dry etching was used to drill holes in the Al layer down to the glass substrate using the patterned ZEP-520 film as a mask. The ICP etching was carried out with BCl_3 (20 sccm) and Cl_2 (10 sccm) gases and RF and ICP power of 100 W for 40 s. The etch selectivity of Al over the resist is 1.18 : 1, leading to an almost complete removal of the mask after etching. Immediately after the ICP treatment, the samples were rinsed in DIW for 5 min to dissolve residual chloride ions. The residual resist was removed from the surfaces with O_2 plasma at an RF power of 50 W and oxygen flow of 15 sccm for 10 min. The diameter of the fabricated holes was measured with a scanning electron microscope and resulted to be equal to approximately 250 nm.

Fabrication of submicron polymer structures at nanoholes

The template molecule (R123, 0.029 mmol), the functional monomer (MAA, 0.23 mmol) and 85 μL of a 60 : 40 (v/v) mixture of AcN/DMSO were placed in a 1.5 mL HPLC vial and shaken for 15 min. After addition of EDMA (0.23 mmol), 2 mg of EY and 20 μL of MDEA, the vial was capped with a rubber septum and the mixture was purged with argon for 5 min. Then 3 μL drops of the mixture were deposited on the fabricated Al nanohole arrays to allow photopolymerization in the metal nanoholes as shown schematically in Fig. 1. A 532 nm-wavelength laser source [5 mW CW532-04 from Roithner Lasertechnik (Vienna, Austria)] was used and the polymerizing light was incident perpendicularly on the metal–glass interface from the bottom

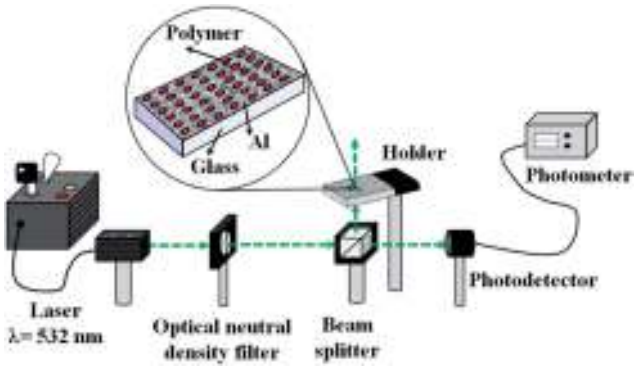

Fig. 1 Scheme of the set up for submicron MIP/NIP structures formation on Al nanohole arrays.

glass substrate. Various exposure times (0.5–16 h) and laser powers (0.72–2 mW) were used. Incident light power was set using different neutral density filters (21 mm dia., Edmund Optics, York, UK) and monitored by a photodetector and a power meter.

Bulk polymers were also synthesized by placing a 300 μL aliquot of the mixture in a 1.5 mL HPLC vial and exposed directly to the laser beam. After polymerization within nanoholes the samples were cleaned with acetone to remove the unreacted solution. Template extraction was achieved by gentle shaking of the polymers, prepared by both polymerization methods, for 2 h in ethanol.

NIPs were prepared as described for MIPs without the presence of the template molecule R123.

Template rebinding studies based on the fluorescence intensity and lifetime

The aluminum samples containing photopolymerized submicron polymer structure arrays were incubated in 25 mL of a 1.0 μM solution of R123 in acetonitrile for 3 h at room temperature. After incubation, the sample was washed twice by dipping it into 5 mL of acetonitrile to eliminate the non-specifically adsorbed R123 and was subject to microscopy investigation. A Horiba (Piscataway, NJ) dynamic fluorescence lifetime imaging microscope (FLIM) was used to characterize the MIP/NIP spots. The setup includes an epifluorescence confocal microscope (Olympus BX51, NY) equipped with three objectives (10×, 20× and 40×) and a trinocular head. The latter is fitted with a 1.4 Mpixel Infinity-3 1UC fluorescence-grade color CCD camera (Lumenera, Ottawa, ON), a thermoelectrically-cooled TBX-04-D single photon detector (Horiba) and a 1600 × 1200 pixel CCD camera (uEye IDS UI-1460, Obersulm, Germany) for bright field image recording. A laser diode (Horiba NanoLED-470LH) was used as an excitation source (463 nm, 900 ps pulse width, 500 kHz repetition rate) together with a 470 nm interference filter (Chroma HQ470/20x, Rockingham, VT) and a 490 nm dichroic mirror (Olympus Q490DCXR)/HQ 500LP band-pass interferential filter combination placed in the cube turret.

All fluorescence decays were measured with a 1000-channel 40 ns window during a fixed time of 5 min. The emission lifetimes were obtained from bi-exponential curve fittings, using the proprietary Horiba hybrid grid-search minimization algorithm (without deconvolution) for stable chi-squared minimization. Measurements (40× objective) were carried out on nine different 20 μm^2 points over the 0.01 mm^2 sampled surface. The pre-exponentially weighted fluorescence lifetimes (eqn (1)) were calculated from the double exponential fit of the decay kinetics profile to eqn (2) and reported throughout the manuscript.

$$\tau_m = \sum_i \frac{B_i}{\sum_i B_i} \tau_i \quad (1)$$

$$\log I(t) = A + B_1 e^{-t/\tau_1} + B_2 e^{-t/\tau_2} \quad (2)$$

Atomic Force Microscopy (AFM) measurements

Topographic images of the nanoholes before and after photopolymerization were acquired with a Bruker AFM IIIa multimode nanoscope (Camarillo, CA). Its FESP probe (Bruker) was made to oscillate at 75 kHz with an elongation constant of 2.8 N m^{-1}. In all cases the images were collected in scan tapping mode.

Optical simulations

Finite-difference time-domain (FDTD) simulations of the optical intensity inside a metallic subwavelength circular hole were carried out using Rsoft software for 532 nm linearly polarized light. The simulation grid encompassed 1 μm in the lateral dimension and 1.5 μm in the vertical dimension, with 5 nm grid spacing in the vicinity of the waveguide. The refractive indexes at 532 nm of glass, aluminum and the photopolymerizable mixture were taken to be 1.523, 0.886–*i*6.253 and 1.381–*i*0.0096, respectively. The real and imaginary parts of the pre-polymerization mixture refractive index were experimentally determined with the aid of a 2WAJ Abbe refractometer (Selecta, Barcelona, Spain) and a Cary 3-Bio (Varian, Palo Alto, CA) spectrophotometer, respectively. A perfectly matched layer boundary condition was used along all three dimensions.

Results and discussion

Subwavelength indicates the use of dimensions below the length of the waves used. Therefore, in order to consider the fabricated Al holes as subwavelength apertures, their diameter (250 nm) should be smaller than the propagation wavelength in the holes (λ/n_{pol}), where λ is the polymerization wavelength and n_{pol} is the refractive index of the medium filling the hole. For polymer mixtures, n_{pol} is typically around 1.4. We chose a polymerization wavelength of 532 nm because (i) the above subwavelength condition is met, (ii) inexpensive solid-state lasers can be employed, and (iii) there exists a well-known photoinitiating system consisting of a mixture of eosin Y (EY) and methyldiethanolamine (MDEA), previously used in holography, laser writing self-guiding polymerization, and plasmon-assisted near field polymerization on Ag nanoparticles,[12,17] that shows good sensitivity at 532 nm.

The pre-polymerization mixture deposited in the nanoholes includes, besides the aforementioned photoinitiating system, ethylene glycol dimethacrylate (EDMA) as a cross-linker (CL) and methacrylic acid (MAA) as a functional monomer (FM). MAA interacts by non-covalent interactions with key functional groups of the model template (R123) allowing generation of high affinity binding sites within the polymer network. As described in the ESI,† the polymer composition was optimized to (i) provide selective recognition of R123 by the imprinted material and (ii) achieve removal of the fluorescent template after polymerization by washing with ethanol, a solvent in which R123 is highly soluble (Table SI.1†). In this way, a mole ratio of 0.5 : 4 : 4, T/FM/CL, was selected for MIP fabrication in the nanoholes. In agreement with the literature reports, such a composition is adequate to maintain the structural integrity of the template-imprinted binding sites in EDMA–MAA systems.[18] The affinity constants and binding capacity of the imprinted and non-imprinted polymers prepared by bulk polymerization were assessed in equilibrium rebinding assays. The experimental data were fitted to a Freundlich isotherm (Table 1 and Fig. 2), as described in the ESI,† resulting in higher values of the weighted average affinity of R123 for the MIP than for the NIP ($K_{MIP} = 21 \pm 3$ mM^{-1} and $K_{NIP} = 8 \pm 1$ mM^{-1}), together with a higher number of binding sites ($N_{MIP} = 41 \pm 3$ μmol g^{-1} and $N_{NIP} = 17 \pm 1$ μmol g^{-1}).[19]

Other dyes structurally related to R123 such as rhodamine 6G and fluorescein showed a markedly lower retention in the MIP (K_{MIP} values of 12 ± 2 mM^{-1} and 11 ± 1 mM^{-1}, respectively), lending further support to the success of the imprinting process. In the case of fluorescein the apparent weighted average affinity in the MIP (11 ± 1 mM^{-1}) was not significantly different from that of R6G (12 ± 2 mM^{-1}) but the total number of binding sites was significantly lower than for this dye (Table 1).

Fig. 3 shows AFM topographic images of the MIP nanostructures generated by photopolymerization on 5 μm-period Al nanohole arrays for different polymerization times. It is clear that local polymerization occurs selectively at the nanohole sites. The nanoholes are almost entirely filled with the polymer after 1 h exposure time at 1.22 mW laser power, as demonstrated by the AFM data. Fig. 4 plots the height (measured from the metal surface) of the polymerized region in the nanoholes as a function of the irradiation time for different incident power values. For each incident light power, the variation of height as a function of the exposure time can be fitted to a η-root function, where η is around 2 (η equals 1.96, 1.85 and 2.17 for 0.72, 1.22 and 2 mW, respectively). This dependence can be theoretically explained through optical numerical simulations as follows.

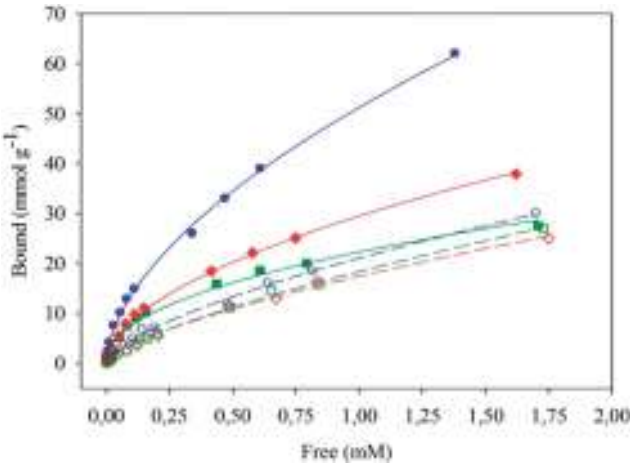

Fig. 2 Equilibrium binding isotherms for the uptake of R123 (blue circles), R6G (red diamonds) and fluorescein (green squares) in the imprinted polymer (solid line) and the non-imprinted polymer (dashed line). Experimental data have been fitted to the Freundlich (FI) isotherm model.

An array period of 5 μm allows nanoholes to behave optically as isolated MSAs because the distance among holes is larger than the propagation length of surface plasmon polaritons at the Al/mixture interface at 532 nm-wavelength (see ESI†). Fig. 5a shows the calculated intensity distribution of 532 nm light impinging on a 250 nm-diameter Al nanohole, fully covered with the pre-polymerization mixture, from the bottom glass substrate. A fraction of the incident light propagates through the aperture – which acts as a metal-clad circular waveguide with a pre-polymerization mixture core – and the transmitted light is diffracted at the aperture edge and radiated to the pre-polymerization medium. The intensity (I) of the diffracted light decays along the distance (z) from the hole output, as shown in Fig. 5b for $\alpha_{mix} = 0.227$ μm^{-1}, where α_{mix} is the absorption coefficient of the pre-polymerization mixture.

This decay results from light radiation from the hole, which leads to an intensity variation as an inverse power of

Table 1 Freundlich fitting parameters, weighted average affinity $\bar{K}_{K_1-K_2}$ and number of sites ($\bar{N}_{K_1-K_2}$) for the selected analyte in the MIP and the NIP (13 data points per isotherm).[19]

Analyte/ polymer	Affinity constant, $\bar{K}_{K_1-K2}$ (mM^{-1})	K_{range} (mM^{-1})	Total number of binding sites $\bar{N}_{K_1-K_2}$ (μmol g^{-1})	Heterogeneity parameter, m	Binding capacity, a (μmol g^{-1} (mM^{-1})^m)	Regression coefficient, r^2
R123/MIP	21 ± 3	0.7–981	41 ± 3	0.57 ± 0.06	51 ± 3	0.999
R123/NIP	8 ± 1	0.6–307	17 ± 1	0.66 ± 0.05	21 ± 1	0.997
R6G/MIP	12 ± 2	0.6–420	26 ± 2	0.54 ± 0.04	29 ± 2	0.996
R6G/NIP	8 ± 1	0.6–275	14 ± 1	0.68 ± 0.07	17 ± 1	0.995
Fluorescein/MIP	11 ± 1	0.6–315	21 ± 2	0.56 ± 0.05	22 ± 2	0.993
Fluorescein/NIP	7 ± 1	0.6–297	13 ± 1	0.71 ± 0.07	18 ± 1	0.998

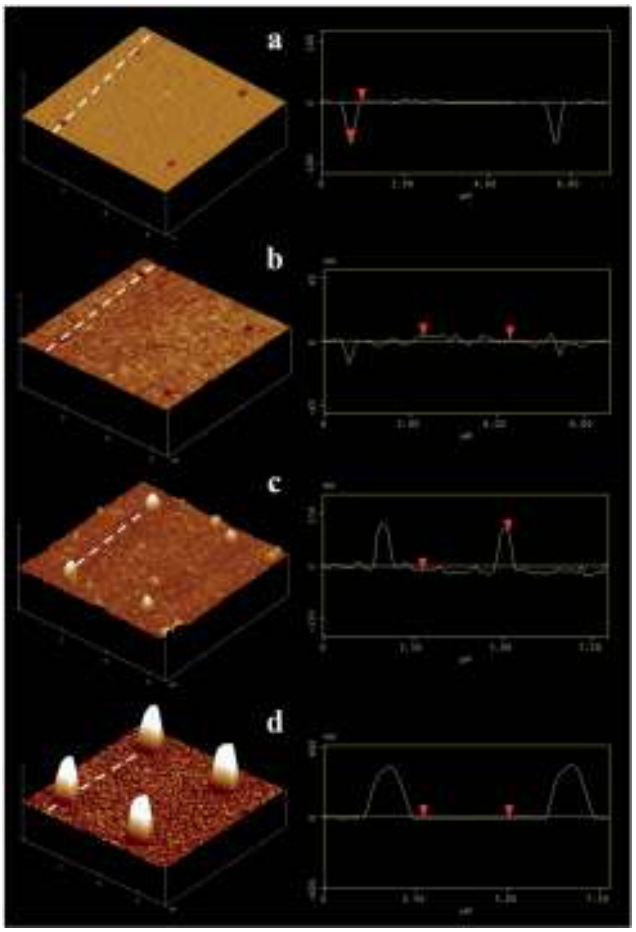

Fig. 3 AFM images and cross-sectional profiles across the corresponding lines of the MIP nanostructures fabricated by photopolymerization, using 1.22 mW 532 nm laser power for different times, on 5 μm-period Al nanohole arrays: (a) 0.5 h; (b) 1 h; (c) 2 h; (d) 16 h irradiation.

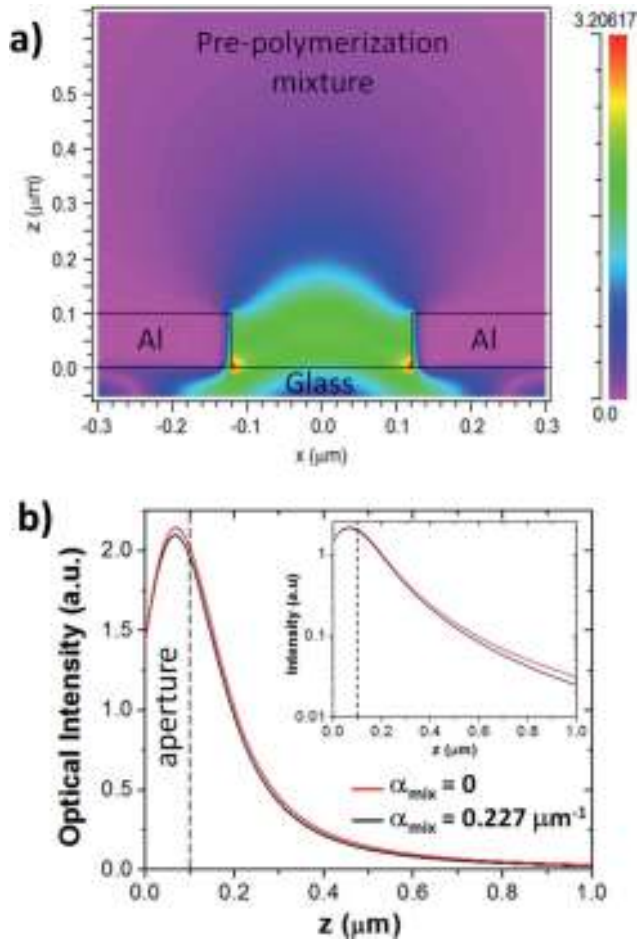

Fig. 5 (a) Calculated intensity distribution of 532 nm light impinging on a 250 nm-diameter Al nanohole, fully covered with the pre-polymerization mixture, from the glass substrate. (b) Intensity profile along the hole axis (z) from the glass surface into the prepolymerization mixture. Inset: logarithmic ordinate–axis representation.

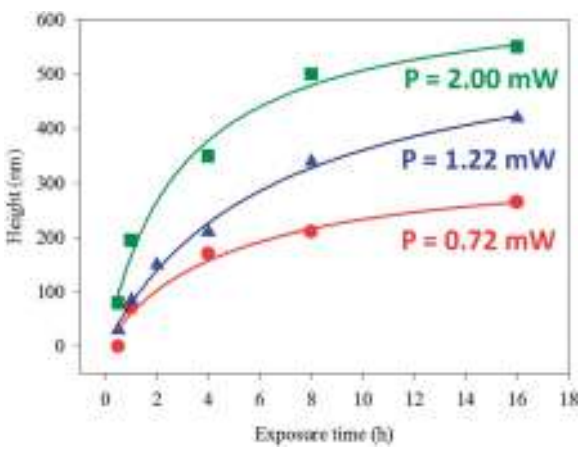

Fig. 4 Effect of the incident light power and exposure time on the height (measured from the Al surface) of the polymerized regions in the nanoholes. Incident power: (a) 2.00 mW (yellow squares), (b) 1.22 mW (blue triangles) and, (c) 0.72 mW (red circles). Polymer heights were measured by AFM (n = 20). Experimental data are fitted to a equation of the form: height = A(exposure time)$^{1/\eta}$, where A and η are fitting parameters.

z (α_{mix} = 0 curve in Fig. 5b), and the medium absorption (intensity decays exponentially with z). According to Fig. 5b, for $z \geq 200$ nm, $I(z, \alpha_{mix} = 0.227\ \mu m^{-1}) \approx I(z, \alpha_{mix} = 0) \sim I_0/z^2$, where I_0 is the intensity at z = 200 nm. Polymerization occurs when the irradiation dose $D(z) = I(z) \times t$ (where t is the irradiation time) is larger than a threshold value $D_{th} = D(z_{th})$. Therefore, the height of the polymerized volume, z_{th}, should vary as $z_{th} \sim (I_0 t/D_{th})^{1/2}$, that is, as the square root of t, in agreement with Fig. 4.

A key issue when investigating the affinity and selectivity of the analyte for a tailored MIP material is to find a sensitive tool to interrogate the binding event.[20] In our case, the problem is aggravated by the small size of the fabricated structures for molecular recognition. The microenvironment of the polymer binding site can alter the photophysical properties of some dyes (*e.g.* rhodamine 6G (ref. 21)) compared to those displayed in solution. In this regard, the selective recognition of the R123 molecule (template) by the imprinted material can be tested by monitoring both the R123 fluorescence intensity and the emission lifetime. Fig. 6 shows a fluorescence image of an array of MIP nanostructures after incubation with 1 μM R123 in acetonitrile.

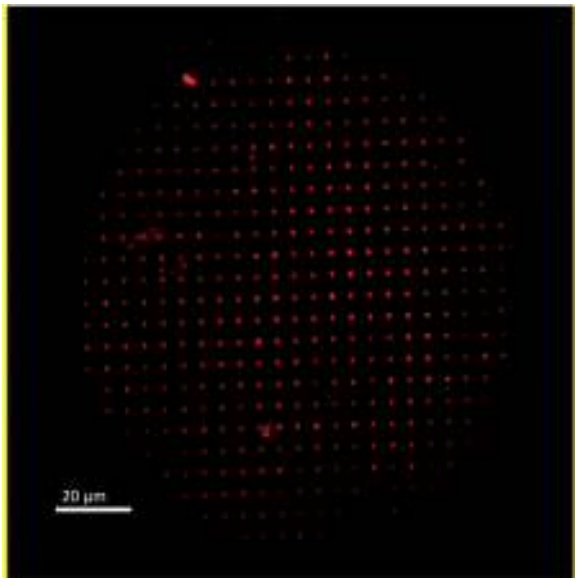

Fig. 6 Fluorescence micrograph of a matrix of submicron MIP structures synthesized on a 5 µm-period Al nanohole array after incubation with R123 (1 µM) in acetonitrile. Polymerization conditions: laser power = 1.22 mW and exposure time = 2 h.

Table 2 Fluorescence lifetime measured under different experimental conditions[a]

Medium	τ_i	τ (ns)
MIP (bulk) after polymerization	τ_1	6.8 ± 0.3 (83 ± 3)
in the presence of R123	τ_2	2.4 ± 0.1 (17 ± 4)
NIP (bulk) after 3 h incubation	τ_1	5.0 ± 0.2 (78 ± 3)
with R123 in AcN	τ_2	1.1 ± 0.2 (22 ± 2)
R123 in the pre-polymerization mixture	τ_1	6.4 ± 0.2 (26 ± 4)
	τ_2	3.3 ± 0.1 (74 ± 1)
Empty nanohole	τ_1	4.2 ± 0.2 (8 ± 2)
	τ_2	0.9 ± 0.1 (92 ± 1)
Al surface (*i.e.* between	τ_1	4.3 ± 0.1 (78 ± 3)
the nanoholes) after	τ_2	2.0 ± 0.1 (22 ± 4)
incubation with R123 in AcN		
R123 in AcN	τ_1	3.9 ± 0.1 (100)
R123 in AcN	τ_1	6.1 ± 0.3 (76 ± 3)
containing 200 mM TFA	τ_2	2.8 ± 0.1 (24 ± 2)

[a] λ_{em} > 500 nm; τ_i and the values in parenthesis (%) represent the emission lifetimes and relative contributions $\left(\%_i = B_i\tau_i \Big/ \sum_i B_i\tau_i\right)$, respectively, of the two components of the fluorescence decay fit ($\log I(t) = A + B_1 e^{-t/\tau_1} + B_2 e^{-t/\tau_2}$); 100% indicates a single-exponential decay. The uncertainty of the measurements is given as the 95% confidence limit, $n = 5$.

The fluorescence lifetime (τ) of R123 was first measured under well-defined conditions, shown in Table 2. The exponential decay ($\tau = 3.9$ ns) in acetonitrile becomes bi-exponential when the dye is dissolved in the pre-polymerization mixture, displaying two components with lifetimes of 6.4 (26%) and 3.3 (74%) ns due to (partial) protonation of the fluorophore by the methacrylic acid monomer. Actually, when trifluoroacetic acid (TFA) is added to the solution of R123 in acetonitrile, the emission decay of the fluorophore becomes bi-exponential (Table 2), with lifetime components of 6.1 (76%) and 2.8 (24%) ns. Moreover, the R123 emission decay acquired immediately after bulk polymerization shows also two components of 6.8 (83%) and 2.1 (17%) ns, pointing out to an increase of the protonated form of R123 due to important hydrogen bonding with the pending methacrylate groups. This interaction is important in the imprinting effect and determines the future recognition of the target analyte in the sample.

To assess the specificity and capacity of the polymer nanostructures to re-bind the R123 molecule, polymer nanostructure arrays of different heights (30, 85, 150 and 420 nm) were tested for their fluorescence decay after various treatments. The results are collected in Fig. 7 (R123 fluorescence intensity) and Table 3 (R123 fluorescence lifetime). Thorough washing of the raw MIP with ethanol leads to a significant decrease of its fluorescence intensity together with a dramatic increase of the contribution of the shorter-lived component (up to 88%). The latter is due to the efficient removal of the R123 dye, leaving the excitation light scattering (and possibly some residual amount of the EY initiator) as the main contribution to the decay. The emission decay parameters observed for the empty nanohole (Table 2) and the NIP (before incubation with R123, Table 3) also support this conclusion. Nevertheless, the emission intensity and lifetime of the largest MIP spots (420 nm high), compared to those observed in the bulk polymer (Table 2), indicate that removal of R123 with ethanol is not complete in this case.

The R123 fluorescence decay parameters demonstrate efficient rebinding of the dye to the MIP. After incubation of the polymer nanostructures with a 1 µM solution of R123 in acetonitrile for 3 h, the emission lifetimes and relative contributions of the dye (Table 3) are similar to those measured in the bulk MIP (Table 2). Again, the contribution of the scattered excitation light to the fluorescence decay slightly reduces the

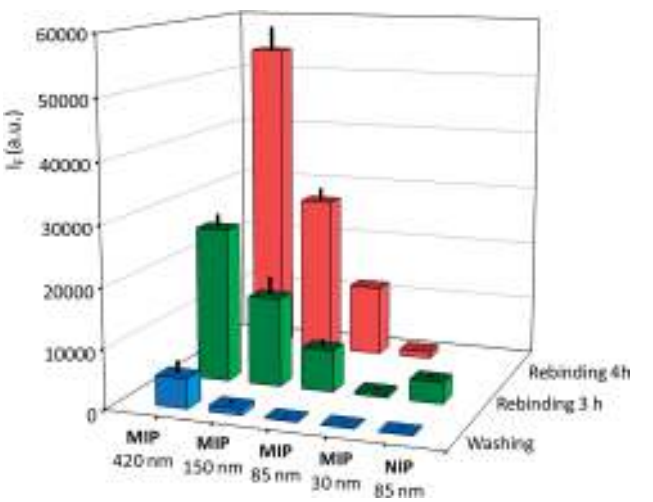

Fig. 7 Fluorescence intensity (I_F) of R123 bound to MIP nanostructures of different heights and to a 85 nm-high NIP, after template extraction (washing) and incubation (re-binding) in acetonitrile (RSD: 2.6–16.8%, $n = 9$).

Table 3 Fluorescence lifetime of R123 bound to the MIPs of different heights, or to the NIP (85 nm-high), after template extraction (washing) and incubation (rebinding) with the fluorescent analyte in acetonitrile[a]

Polymer	Height (nm)	τ_i	τ (ns) (after washing)	τ (ns) (after 3 h rebinding)	τ (ns) (after 4 h rebinding)
MIP	420	τ_1	5.5 ± 0.3 (82 ± 3)	6.4 ± 0.1 (90 ± 2)	6.3 ± 0.1 (88 ± 4)
		τ_2	2.4 ± 0.3 (18 ± 2)	2.7 ± 0.2 (10 ± 3)	2.5 ± 0.1 (12 ± 3)
MIP	150	τ_1	4.7 ± 0.3 (14 ± 3)	6.4 ± 0.2 (92 ± 2)	6.2 ± 0.1 (91 ± 2)
		τ_2	2.3 ± 0.2 (86 ± 3)	2.7 ± 0.2 (8 ± 2)	2.5 ± 0.1 (9 ± 1)
MIP	85	τ_1	4.5 ± 0.2 (15 ± 2)	6.3 ± 0.3 (88 ± 4)	6.1 ± 0.1 (80 ± 3)
		τ_2	2.3 ± 0.2 (85 ± 3)	2.3 ± 0.1 (12 ± 3)	2.3 ± 0.1 (20 ± 3)
MIP	30	τ_1	4.4 ± 0.2 (12 ± 4)	4.9 ± 0.5 (76 ± 5)	4.7 ± 0.2 (79 ± 4)
		τ_2	2.0 ± 0.1 (88 ± 3)	2.1 ± 0.1 (24 ± 3)	1.9 ± 0.1 (21 ± 3)
NIP	85	τ_1	4.2 ± 0.1 (9 ± 2)	5.0 ± 0.1 (73 ± 4)	
		τ_2	0.8 ± 0.1 (91 ± 2)	0.9 ± 0.1 (27 ± 3)	

[a] τ_i and the values in parenthesis (%) represent the emission lifetimes and relative contributions $\left(\%_i = B_i\tau_i \Big/ \sum_i B_i\tau_i\right)$, respectively, of the two components of the fluorescence decay fit ($\log I(t) = A + B_1 e^{-t/\tau_1} + B_2 e^{-t/\tau_2}$); the uncertainty of the measurements is given as the 95% confidence limit, $n = 9$.

observed lifetime and relative contribution of the longest-lived component for the smallest (30 nm-high) polymer spot. Further incubation of the MIPs with the template for an additional hour demonstrates that a higher amount of the latter can still be hosted: the emission intensity doubles that of the 3 h incubated samples (Fig. 7), but their corresponding emission lifetimes do not change regardless of the polymer spot size (Table 3).

The measured fluorescence intensity increases with the height of the polymer regions generated at the nanoholes. This fact is due to a larger amount of polymer-bound R123 after incubation in the higher MIP spots. Moreover, the emission intensity of the 85 nm-high MIP after incubation for 3 h (7000 ± 1000 a.u.) is twice as large as that observed for the NIP incubated with R123 under the same conditions (3700 ± 400 a.u.), demonstrating a stronger binding of the template to the molecularly imprinted material.

The preference of R123 for binding to the MIP over the NIP is also demonstrated by comparison of the fluorescence decay of the polymer-bound dye and that of the green light collected by the confocal microscope focused on the aluminum surface between the nanohole patterns. The measured bi-exponential emission decay parameters in the latter case (4.35 ns, 78%, and 2.01 ns, 22%, Table 2) show that indeed some amount of highly fluorescent dye becomes attached to the metal surface after the 3 h incubation; however, its fluorescence decay is faster than that observed for the MIP-bound dye (6.39 ns, 90%, and 2.68 ns, 10%, Table 3). This lifetime shortening might be due to a metal-induced effect.[22] The aluminum-bound R123 emission decay parameters are identical to those measured for the smallest MIP spot (30 nm, Table 3) due to the fact that the microscopy observation spot (10 μm diameter) is larger than the polymer-filled hole (250 nm-diameter); in this situation, the vast majority of the collected fluorescence comes from the dye molecules outside the hole. A similar situation (5.0 ns, 73%, and 0.9 ns, 27%, Table 3) occurs when measuring the NIP spot after incubation with R123, demonstrating that it has not re-bound a significant amount of the dye.

Conclusions

We have fabricated for the first time sub-micron lateral resolution MIP patterns by photoinduced local polymerization within MSAs. The size of the photopolymerized MIP features can be controlled by the dose of 532 nm radiation. By using R123 as the fluorescent model template, we have demonstrated the recognition capability of the MIP nanostructures, which has been evaluated by FLIM with single photon timing measurements. Lifetime measurements allow elucidating the affinity of the fluorescence template rebinding to imprinted nanomaterials. The presented MIP nanostructure fabrication method is simple and particularly suitable for mass production of biomimetic sensor arrays that might be used in the future for cost-effective, selective, sensitive lateral-flow assays with hand-held devices in environmental, clinical and food analysis.

Acknowledgements

The authors gratefully acknowledge financial support from MINECO (TEC2010-10804-E, CTQ2012-37573-C02). J. L. Urraca thanks the Moncloa Campus of International Excellence (CEI) for a postdoctoral contract.

Notes and references

1 *Molecular Imprinting, Topics in Current Chemistry*, ed. K. Haupt, Springer, Berlin Heidelberg, 2012, vol. 325.
2 Y. Fuchs, O. Soppera and K. Haupt, *Anal. Chim. Acta*, 2012, **717**, 7–20.
3 S. Guillon, R. Lemaire, A. Valvanuz Linares, K. Haupt and C. Ayela, *Lab Chip*, 2009, **9**, 2987–2991.
4 Y. Fuchs, A. V. Linares, A. G. Mayes, K. Haupt and O. Soppera, *Chem. Mater.*, 2011, **23**, 3645–3651.

5 P. G. Conrad II, P. T. Nishimura, D. Aherne, B. J. Schwartz, D. Wu, N. Fang, X. Zhang, M. J. Roberts and K. J. Shea, *Adv. Mater.*, 2003, **15**, 1541–1544.
6 D. Forchheimer, G. Luo, L. Montelius and L. Ye, *Analyst*, 2010, **135**, 1219–1223.
7 S. Carrasco, V. Canalejas-Tejero, F. Navarro-Villoslada, C. A. Barrios and M. C. Moreno-Bondi, *J. Mat. Chem. C*, 2014, **2**, 1400–1403.
8 *Surface-Enhanced Raman Scattering – Physics and Applications, Topics in Applied Physics*, ed. K. Kneipp, M. Moskovits and H. Kneipp, Springer, Berlin Heidelberg, 2006, vol. 103.
9 T. Lohmüller, L. Iversen, M. Schmidt, C. Rhodes, H. L. Tu, W. C. Lin and J. T. Groves, *Nano Lett.*, 2012, **12**, 1717–1721.
10 J. Aizenberg, J. A. Rogers, K. E. Paul and G. M. Whitesides, *Appl. Phys. Lett.*, 1997, **71**, 3773–3775.
11 A. Sundaramurthy, P. J. Schuck, N. R. Conley, D. P. Fromm, G. S. Kino and W. E. Moerner, *Nano Lett.*, 2006, **6**, 355–360.
12 C. Deeb, C. Ecoffet, R. Bachelot, J. Plain, A. Bouhelier and O. Soppera, *J. Am. Chem. Soc.*, 2011, **133**, 10535–10542.
13 T. W. Ebbesen, H. J. Lezec, H. F. Ghaemi, T. P. Thio and A. Wolff, *Nature*, 1998, **391**, 667–669.
14 M. J. K. Klein, M. Guillaumée, B. Wenger, L. Andrea Dunbar, J. Brugger, H. Heinzelmann and R. Pugin, *Nanotechnology*, 2010, **21**, 205301 (7 pp).
15 M. Foquet, K. T. Samiee, X. Kong, B. P. Chauduri, P. M. Lundquist, S. W. Turner, J. Freudenthal and D. B. J. Roitman, *J. Appl. Phys.*, 2008, **103**, 034301.
16 M. J. Levene, J. Korlach, S. W. Turner, M. Foquet, H. G. Craighead and W. W. Webb, *Science*, 2003, **299**, 682–686.
17 O. Soppera, S. Jradi and D. J. Lougnot, *J. Polym. Sci., Part A: Polym. Chem.*, 2008, **46**, 3783–3794.
18 S. Sellergren and A. J. Hall, Fundamental aspects on the synthesis and characterization of imprinted network polymers in *Molecularly imprinted polymers: man-made mimics of antibodies and their applications in analytical chemistry*, ed. Sellergren, S., Elservier Sci., The Netherlands, 2001, p. 35.
19 A. M. Rampey, R. J. Umpleby, G. T. Rushton, J. C. Iseman, R. N. Shah and K. D. Shimizu, *Anal. Chem.*, 2004, **76**, 1123–1133.
20 S. Subramanian Suriyanarayanan, P. J. Cywinski, A. J. Moro, G. J. Mohr and W. Kutner, *Top. Curr. Chem.*, 2012, **325**, 165–266.
21 W. Holzer, H. Gratz, T. Schimitt, A. Penzkofer, A. Costela, I. García-Moreno, R. Sastre and F. J. Duarte, *Chem. Phys.*, 2000, **256**, 125–136.
22 *Metal-Enhanced Fluorescence*, ed. C. D. Geddes, John Wiley & Sons, Inc., Hoboken, New Jersey, 2010.